A Narrowband 3-D Printed Invar Spherical Dual-Mode Filter With High Thermal Stability for OMUXs

Qian, Lu; Wang, Yi; Li, Sheng; Mohamed, Abd El Moez A.; Attallah, Moataz M.; Skaik, Talal; Booth, Paul; Pambaguian, Laurent; Espana, Cesar Miquel; Mart, Petronilo

DOI:
10.1109/TMTT.2022.3152795

A Narrowband 3-D Printed Invar Spherical Dual-mode Filter With High Thermal Stability for OMUXs

Lu Qian, *Graduate Student Member, IEEE*, Yi Wang, *Senior Member, IEEE*, Sheng Li, Abd El-Moez A. Mohamed, Moataz M. Attallah, Talal Skaik, Paul Booth, Laurent Pambaguian, César Miquel España, and Petronilo Martín-Iglesias

***Abstract*—A 3-D printed narrowband bandpass filter based on spherical dual-mode resonators is presented in this paper. It is designed for output multiplexers using high-*Q* spherical dual-mode resonators. Realization is by Laser Powder Bed Fusion (PBF) technology of Invar alloy chosen for its low coefficient of thermal expansion (CTE). Using PBF circumvents the alloy's manufacturability issues associated with its hardness in machining and free forming. Compared with polymer-based vat photopolymerization technology, PBF allows for direct metal manufacture of complex monolithic microwave components with better thermal-mechanical properties and higher power handling capability. Using Invar can further help achieve high temperature stability of the filter in high-power operation. To demonstrate the proposed solution, detailed thermal-RF test at different temperatures was carried out. The experimental results of a 0.47% 4th-order silver-plated Invar filter with two transmission zeros verify the design and manufacturing. An insertion loss of 1 dB and an effective temperature coefficient of less than 2 ppm/K were achieved.**

***Index Terms*—3-D printing, high-power filter, Invar, novel materials, output multiplexer, spherical resonators**

I. Introduction

HIGH-POWER filters and multiplexers for space applications require high temperature stability due to their large operation temperature ranges as well as the power-induced self-heating effect. Among these devices is the output multiplexer (OMUX), one of the most complex and specialized passive components, also with the most stringent requirement for temperature stability. This is partly because of the narrow channel bandwidth (e.g. 36 or 54 MHz in X and Ku band) and partly because of the tight frequency and distance spacing between the channels. In fact, contiguous channel configurations are not uncommon. This leaves almost no bandwidth margin to allow for any frequency drift. To achieve a sufficiently high temperature stability, there are two well established temperature compensation techniques. One is to build the filter using Invar material with very low coefficient of thermal expansion (CTE of 0.5~2.0 ppm/K) [1]. The other is to build the filter from the favorably light aluminum but using external compensation mechanisms to achieve effective thermal compensation [2]. This complicates the assembly. Despite the attractively low CTE, Invar is not an easy material to work with for its high density and hardness in machining. Moreover, some essential mechanical features such as the straps and brackets will degrade the thermal handling capacity of the channel filter [1]. In this work, a new alternative fabrication route for Invar-based filters is demonstrated using additive-manufacturing (AM).

Different from the conventional subtractive process, AM (known also as 3-D printing) offers the flexibility and capability by selectively building material in layer-upon-layer fashion to form complex geometries monolithically, which is either impossible or too complicated for conventional machining [3]–[5]. When using INVAR, design could be geared toward higher RF performances and reduce cost for machining. AM also provides more design freedom for multi-objective topological optimization of the weight, mechanical and thermal properties. In this work, we will demonstrate a filter with spherical resonators, conformal cavity walls and modified flanges, built in one single piece using laser powder bed fusion (L-PBF) process from Invar powders. More specifically, the selective laser melting (SLM) technique is employed.

Most of the OMUX channel filters are implemented using dual-mode resonators for compactness and ease of layout

This work was supported by the GSTP program in the frame of the ESA contract 4000131423/20/NL/FE "Next Generation Temperature Compensated High Power Filters Based on Novel Materials".

L. Qian, T. Skaik, and Y. Wang are with School of Engineering, University of Birmingham, Birmingham, B15 2TT UK (e-mail: lxq961@student.bham.ac.uk, T.F.Skaik@bham.ac.uk, Y.Wang.1@bham.ac.uk).

S. Li, A. Mohamed, and M. Attallah are with School of Metallurgy and Materials, University of Birmingham, Birmingham, B15 2TT UK. (e-mail: S.Li.2@bham.ac.uk, A.A.M.A.Hussein@bham.ac.uk, M.M.Attallah@bham.ac.uk).

P. Booth is with the Airbus Defence and Space Ltd, Stevenage SG1 2AS UK, (e-mail: Paul.Booth@airbus.com).

L. Pambaguian, C. España, P. Martín-Iglesias are with the European Space Agency, Keplerlaan 1, 2201 AZ Noordwijk, Netherlands, (e-mail: Laurent.Pambaguian@esa.int, Cesar.Miquel.Espana@esa.int, Petronilo.Martin.Iglesias@esa.int).

especially when the channel number is high [6]. Among them, cylindrical high-Q TE_{11N} dual-mode resonators are the most widely used [7], [8]. However, they are normally manufactured cavity-by-cavity or in a split-block fashion. The separate cavities and the split-blocks require extra flanges and screws for assembly. Using AM, one can manufacture not only the Invar filters but also the attached mechanical features (such as brackets and straps) monolithically, with no or reduced interconnection and assembly. This can further translate to reduced mass and less passive intermodulation when the devices work with multiple carriers. In addition, unconventional geometric features are made possible by AM, such as: self-supportive spherical or elliptic cavities for enhanced RF performance, rounded corners for reduced field concentration and ease of plating, and waffle structures for local mechanical reinforcement.

Although the SLM of Invar material [9] has been well studied, we have not found any SLM Invar filters reported in the open literature, except for brief mention in marketing literature from commercial providers such as Swissto12. It is very important to note that majority of the previously demonstrated 3-D-printed filters are of relatively wide band (most larger than 2%) [10], [11], unsuitable for OMUXs. These filters are also much less sensitive to fabrication tolerance than the narrowband dual-mode filter we chose to build and demonstrate. A spherical dual-mode resonator filter with 0.47% fractional bandwidth is presented in this work. A polymer version of the spherical dual-mode resonator using stereolithography technology was first reported in [12]. Holes were added to the structure to facilitate plating. The bandwidth of the filter was over 3%. The high thermal expansion, low power handling, knotty EMC problems with the plating holes, and potential issues related to mechanical loads hinder the polymer-based filters from being used in higher-power OMUXs of real-world satellite payloads.

In this paper, the mechanical properties, as well as the RF and thermal stability performance of SLM Invar resonators and filters are demonstrated. Comparison with an aluminum-copper alloy is done. The manufacturing parameters and the coating process are discussed.

II. Spherical Dual-mode Filter Design

A spherical dual-mode fourth-order filter with a quasi-elliptic response and two transmission zeros is adopted here. Fig. 1(a) shows the configuration of the proposed filter. It consists of two spherical resonators which are joined by a cross shaped iris. Two WR-90 waveguides serve as the feeding ports. Each resonator supports a pair of orthogonally polarized TM_{101} resonance modes. Table I shows a comparison between the used spherical resonator and the common dual-mode cavity resonators in terms of the simulated unloaded quality factor (Q_u) and the corresponding physical dimensions, where all resonators operate at 11.5 GHz. All EM-simulations were performed using the Computer Simulation Technology (CST) Studio Suite, and all cavity walls were assumed to be smooth silver with electrical conductivity of 6.302×10^7 S/m. From this

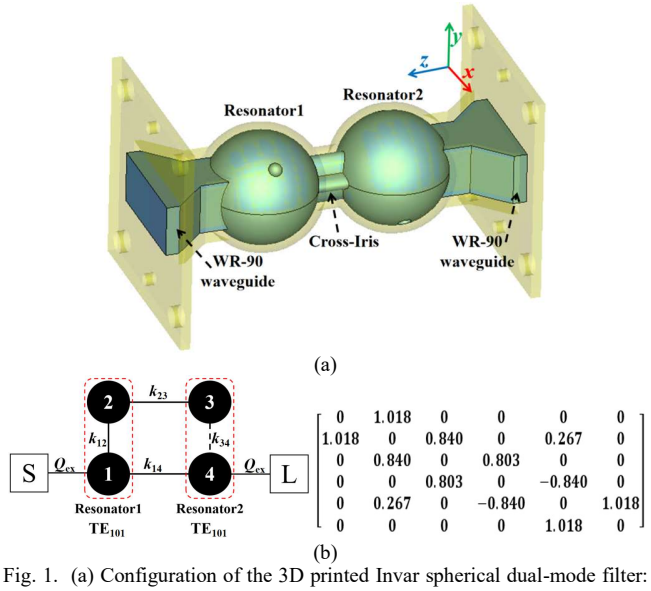

Fig. 1. (a) Configuration of the 3D printed Invar spherical dual-mode filter: (yellow: the metallic wall; blue: the internal air-model). (b) Coupling topology and normalized coupling matrix. (Solid line: Positive coupling, Dash line: Negative coupling)

table, it can be seen that the spherical dual-mode resonator exhibits significant advantages over the others. It has the highest Q_u among the dominant modes (TE_{101}, TE_{111}, TM_{101}) and shows considerably reduced size over other higher modes.

TABLE I
Comparison of Different Types of Cavity Resonators.

Resonator	Mode	Q_u	Dimensions (mm)
Rectangular	TE_{101}	7936	22.86 (L) × 10.16 (W) × 15.87 (H)
	TE_{102}	9910	22.86 (L) × 10.16 (W) × 31.73 (H)
	TE_{103}	10710	22.86 (L) × 10.16 (W) × 47.60 (H)
Cylindrical	TE_{111}	11870	27.18 (D) × 15.68 (H)
	TE_{112}	17149	27.18 (D) × 31.36 (H)
	TE_{113}	19873	27.18 (D) × 47.03 (H)
Spherical	TM_{101}	14015	22.80 (D) × 22.80 (D)

L, W, H, D, denote length, width, height, and diameter of the resonators.

The filter is designed to have a center frequency of 11.483 GHz, bandwidth of 54 MHz, and passband return loss of 20 dB. The coupling topology is shown in Fig. 1(b), where the cross coupling between mode 1 and 4 is introduced to generate two symmetrical transmission zeros at 11.438 GHz and 11.528 GHz to improve the frequency selectivity. From [13], the external quality factor and non-zero coupling coefficients can be calculated: $Q_{ex} = 205.7$, $k_{12} = -k_{34} = 0.840$, $k_{23} = 0.803$, and $k_{14} = 0.267$.

Fig. 2 illustrates the YZ-plane sectional view of the filter and some critical coupling structures. The two black arrows indicate the electric field (E-field) direction of mode 1 and mode 4. The dash lines denote three XY-plane cross sections (XY-1, 2, 3) with key coupling structures to be detailed later in Fig. 3 and 4. The first and third one is located at the middle of the two spherical cavities whereas the second one is at the middle of the

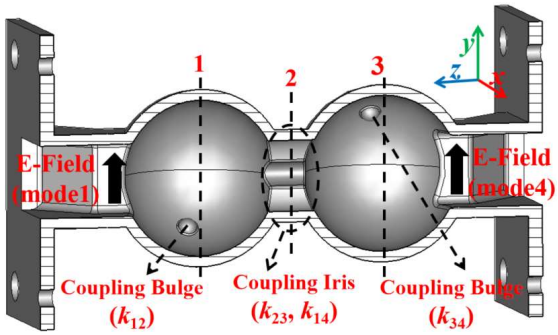

Fig. 2. Section view showing the internal structures. (Two red solid arrows indicate E-field direction, and three red dash lines indicate the position of three *XY*-plane cross sections with critical coupling structures).

cross-iris.

The inset in Fig. 3(a) displays the cross section XY-1 and XY-3. They are not strictly circular but elliptical with a width-height ratio close to 1. The horizontal and vertical radius of each spherical cavity are labelled as R_1, R_2, R_3 and R_4. By changing them, the frequency of each mode can be tuned. The intra-resonator coupling (k_{12} and k_{34}) between the two orthogonal modes can be further controlled by a pair of round bulges at +/− 45° directions. The purpose for adding a pair of coupling bulges rather than just one in each cavity is to reduce the impact on the polarization orthogonality between the two TM resonance modes. Compared with the commonly used coupling stubs [12], the round bulge is easier to be printed and integrated with the spherical cavity. Positioning the coupling bulges at +/- 45° enables the coupling k_{12} and k_{34} to be out of phase and hence achieves the required coupling topology. Fig. 3(a) shows the phase responses of the transmission coefficient where the +/- 45° coupling bulges exhibit opposite phase. The coupling strength is determined by the radius of the coupling bulges Br_1 or Br_2, as presented in Fig. 3(b).

The inter-resonator and cross coupling are realized by the cross shaped iris between two cavities where the horizontal aperture is for the cross coupling k_{14} and the vertical aperture is for the main line coupling k_{23}, as indicated in Fig. 4(a). In this design, the thickness of the iris t is deliberately increased to allow an enlarged iris opening. This is an important feature because it not only eases the printing process but also facilitates the subsequent surface treatment (polishing and coating), when either polishing agents or an electrode needs to be inserted into the cavities. Fig. 4(b) shows the variation of the coupling coefficient versus the width of coupling aperture l for different thicknesses t. To achieve the same level of coupling, a thicker iris will allow an increased l. It is also shown that the curve

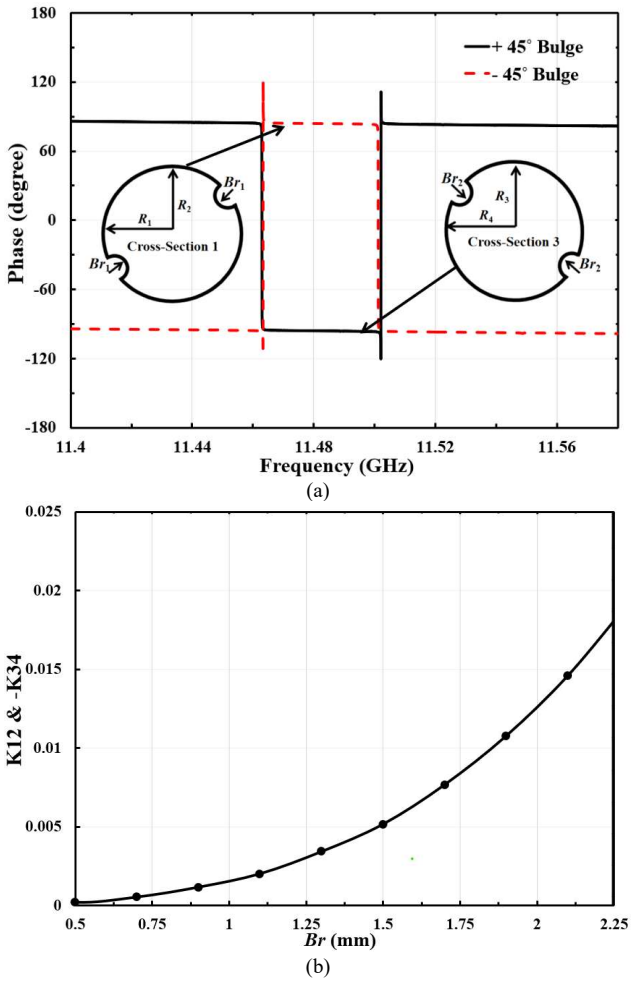

Fig. 3. (a) Phase response of the transmission coefficient of the intra-resonator coupling with insets showing the corresponding structures and dimensions. (b) Extracted coupling coefficient versus the radius of the coupling bulges *Br*. The final dimensions in millimeter are: R_1= R_4 = 11.025, R_2 = R_3 = 10.954, R_1/R_2 = 1.0065, Br_1 = Br_2 = 1.345.

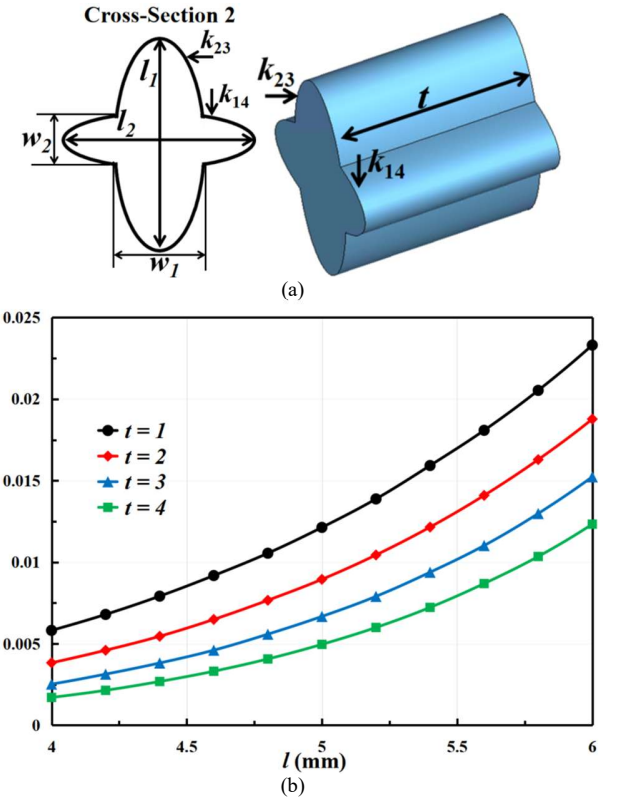

Fig. 4. (a) The inter-resonator and cross coupling structures with key dimensions. (b) Extracted coupling coefficient versus the dimension l (w = 2 mm) with varying t. The final dimensions in millimeter are t = 4.3, l_1 = 5, w_1 = 2.33, l_2 = 4.25, w_2 = 2.

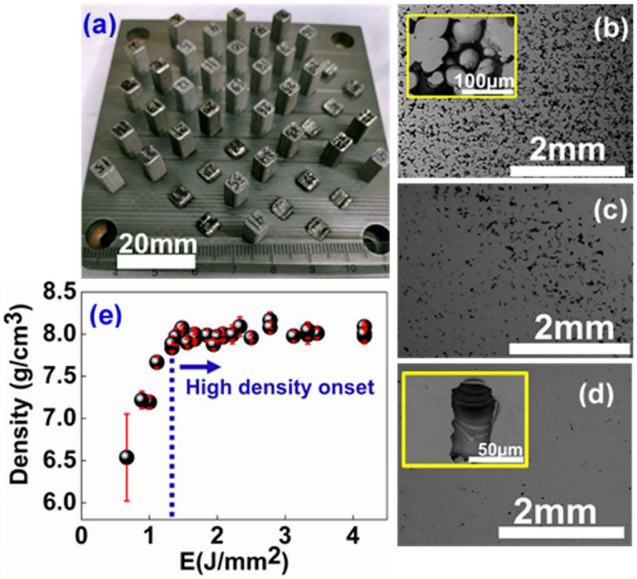

Fig. 5. (a) The as-printed coupons with different laser energy density E on top of a steel substrate, (b) (c) (d) SEM micrographs of the coupons built with E = 0.8, 1.1 and 1.4 J/mm^2, respectively, which show the influence of laser process parameters on densification mechanism. The inset shows the respective microstructural defects, and (e) the influence of laser process parameters on the Archimedes density.

representing the thicker iris has a gentler slope. This means the thicker iris reduces the sensitivity to the fabrication tolerance as an added benefit. The wider and longer iris would have a negative impact on the spurious performance. However, both measurement and simulation show that there is no spurious passband over the whole X band from 8.2 to 12.4 GHz.

III. Material, Manufacture and Coating

The Invar filter samples were 3D printed from a pre-alloyed spherical powder on top of a steel substrate with SLM additive manufacturing technique using a Concept Laser M2 Cusing system. In order to achieve maximum bulk microstructure density, a laser parametric study was performed first on 5 mm × 5 mm × 7 mm coupons as shown in Fig. 5(a), using the laser processing window parameters given in Table II and with a constant powder layer thickness of 30 μm. The heat input was represented in terms of the laser energy density (E = *Laser-Power*/*Scan-Speed*/*Scan-Spacing*) [14]. The scanning electron microscope (SEM) micrographs in Fig. 5(b)-(d) show the influence of E on the microstructure's density evolution. It is observed that the coupons built with $E \leq 1.0$ J/mm^2 show porous microstructure with unfused defects (un-melted particles within the pores) as seen in Fig. 5(b), leading to low density. The monotonic increase in E decreases the lack-of-fusion defects and increases the degree of consolidation, as shown in Fig. 5(c) and (d), leading to a dense material when the laser energy

TABLE II
Investigated Range of Processing Parameters.

Material	Laser power/P (W)	Scan speed/V (mm/s)	Scan spacing/h (mm)	Energy density/E (J/mm^2)
Invar	150-350	800-2500	0.06-0.09	0.6-7.3
A20X	360	1500	0.15	1.6

TABLE III
Mechanical Properties of the SLM Invar and A20X Alloy.

Material	Density (g/cm^3)	E* (GPa)	$\sigma_{0.2}$ (MPa)	σ_{UTS} (MPa)	δ (%)
A20X-AF#	2.85	72.8/75.5	303/313	398/390	9.8/9.6
Invar-AF [9]	8.1	-	398/353	510/422	15/3

*E: Elastic modulus; $\sigma_{0.2}$: Yield strength; σ_{UTS}: Ultimate tensile strength; δ: Elongation. #AF: As-fabricated.

density is between $1.4 \leq E \leq 4.2$ J/mm^2. However, the higher E values in this range lead to evaporation that creates pores within the builds as seen in Fig. 5(d). Also, the high E parameters might cause over-melting, rough downward surface, and distortion. The consolidation behavior is also represented by the Archimedes density measurements in Fig. 5(e), where all coupons built with $1.4 \leq E \leq 4.2$ J/mm^2 show fairly constant density with an average value of 8.0 g/cm^3. In order to achieve reasonably high density as well as good surface finishing, the parameter chosen to manufacture the part is 1.4 J/mm^2, which is the minimum E required to reach the high-density regime. The estimated porosity fraction is 2.3 ± 0.15%. It is worth mentioning that all builds beyond E = 4.2 J/mm^2 failed as the extremely high E value leads to higher thermal stresses [15].

An aluminium-copper alloy (A20X) sample was also 3D printed and used as a benchmark as its CTE value is similar to the aluminium alloy used for space application. The A20X sample was fabricated using a SLM500HL printer with the processing parameter given in Table II.

Table III compares the SLM Invar and SLM A20X in terms of their mechanical properties. Where two values are provided, they correspond to the horizontal/vertical building directions, respectively. This measurement was carried out by Deben 500 tensile testing machine using 2 mm × 2 mm flat dogbone samples.

The printing direction is parallel to the propagation direction of the microwave components, as shown in Fig. 6. No internal support structures are required. The design has considered several features to facilitate SLM manufacturing. The spherical cavities are self-supportive during the printing. The inter-cavity and input/output irises alleviate overhangs of greater than 45°. The feed waveguide is tapered to avoid flat ceilings. The waveguide flange is modified (see the photo in Fig. 6) to alleviate stress-induced bending as well as to reduce the weight. The as-printed samples were cut off the substrates via EDM and the flange surface was mechanically ground to improve its smoothness. Post polishing was done by a Sharmic vibration polishing machine with 3 mm size ceramic particle media. The polishing process takes 6 hours, and the samples are then ultrasonically cleaned with ethanol for 10 min and dried in oven at 100 °C before further testing.

The SLM Invar filter was electroplated with silver. Fig. 6 shows the photography of the Invar filter after surface coating. To encourage coating on the inside, part of the external surface was masked during plating. An anode was inserted through the filter. This necessitates large enough irises in the design especially for narrow band filters. The roughness of the internal

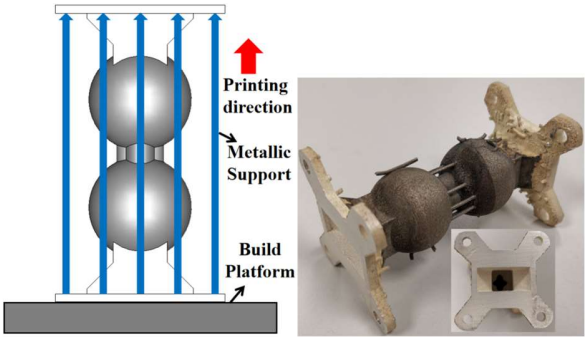

(a) (b)

Fig. 6. (a) Diagram showing the printing direction; (b) Photo of the Invar filter after silver plating.

surface is believed to have some adverse impact on the quality of silver plating. It is worth mentioning that silver plating on machined Invar is a well-tested and used process in general. However, what is less known is the quality of coating on the internal surface of a semi-closed, monolithic, 3D-printed part like the cavity filter. This is worth further investigation and research.

IV. Measurement and Discussion

To evaluate the printing quality and the thermal stability of the printed Invar components, a thermal-RF measurement was performed. This test was carried out using an in-house built experimental setup where a pair of thermal isolators are used [16].

A dimpled spherical single-mode resonator [17] was first measured. To provide a benchmark and the first-order indication of the dimension accuracy of the as-printed sample,

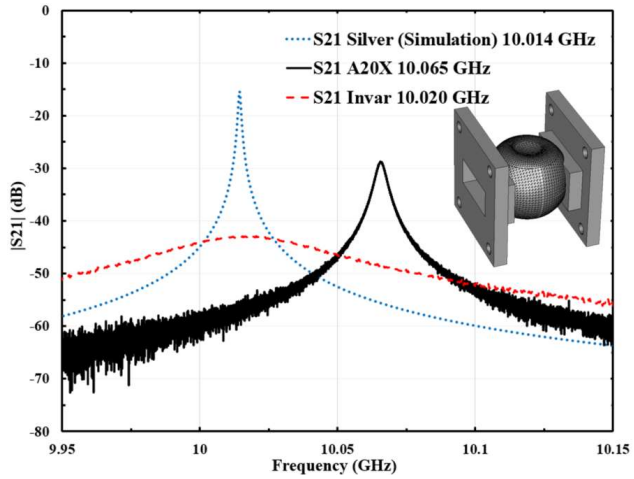

Fig. 7. Measured resonance curves at room temperature with inset showing the dimpled spherical single-mode resonator.

an A20X and an Invar resonator were first tested at room temperature (~20 °C). As shown in Fig. 7, both samples have a slightly higher resonance frequency than expected from the simulation, which is partly due to the shrinkage during the printing process. From the transmission response in Fig. 7, the Q_u and the corresponding effective electrical conductivity can be further extracted, as presented in Table IV.

TABLE IV
Measurement Result Summary of The Resonators.

Material	Q_U @20 °C	Effective conductivity ($\times 10^7$S/m)	Effect. temp. coefficient (ppm/K)
Invar	167	0.0015	1.85
A20X	4057	0.778	21.7

Next, the operating temperature was raised up to 160°C at an interval of around 20°C. The transmission responses at each point were measured after a stabilization time of 30-40 minutes. Fig. 8 shows the measured resonance curves as a function of temperature for both resonators. It is apparent that the frequency variation of the Invar resonator is negligible comparing to the A20X resonator. To establish a correlation between the frequency shift and the CTE, we define the 'effective temperature coefficient' of the resonator as

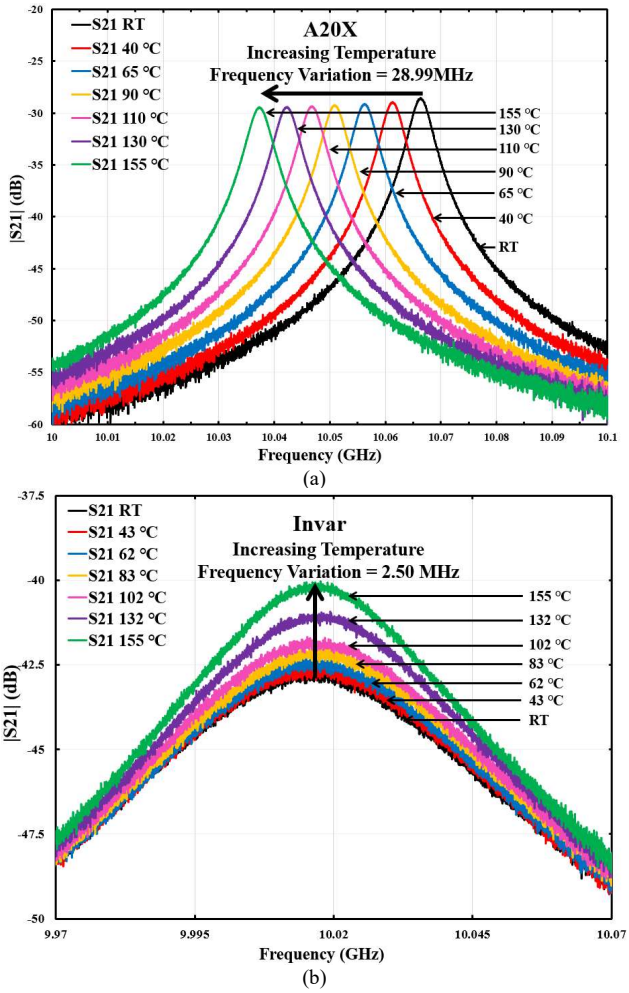

Fig. 8. Measured resonance curves as a function of temperature. (a) A20X resonator. (b) Invar resonator.

$\mathrm{d}(\Delta f/f)/\mathrm{d}T$. It has the same unit of ppm/K as the CTE of the materials. The start and end temperature are used to extract this coefficient. The results are summarized in Table IV. The Invar resonator has a very low thermal expansion of 1.85 ppm/K. Its Q_u increased slightly with temperature. As expected, the Invar resonator has extremely low Q_u. It requires surface-coating to

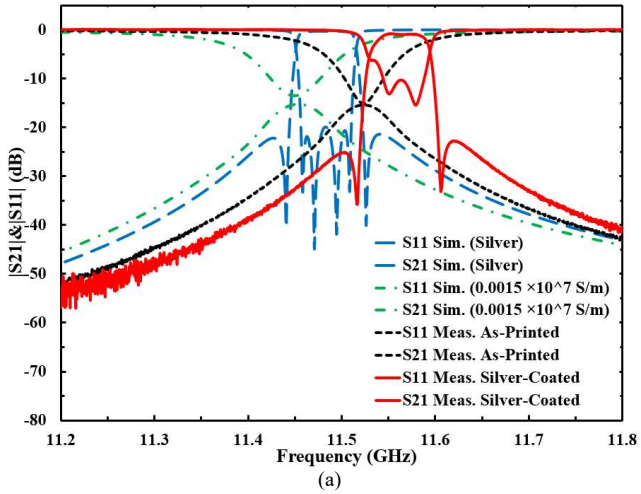

(a)

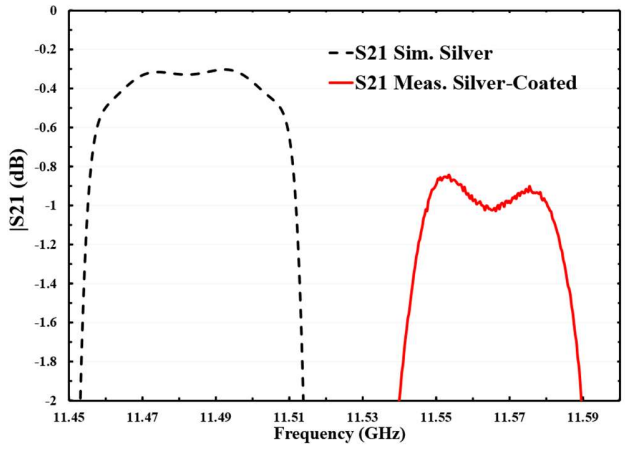

(b)

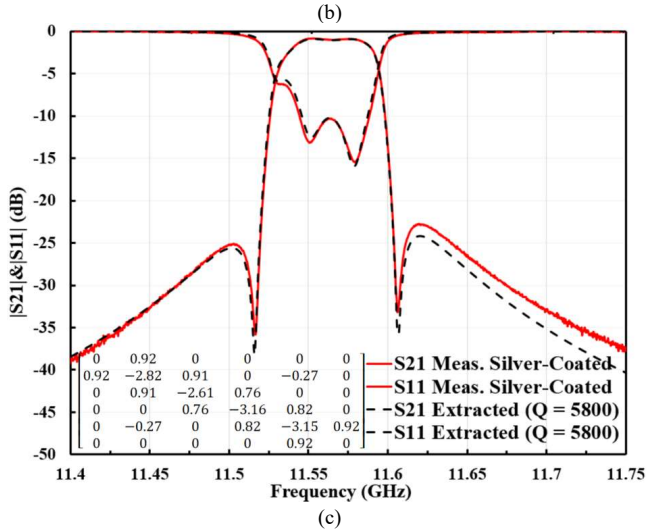

(c)

Fig. 9. (a) Measurement (solid lines) and simulation (dashed lines) results of the 3D printed Invar filter. (b) The enlarged view of S_{21} responses over the passband. (c) comparison between the measured results and the filter response from the extracted coupling matrix (see the inset).

improve its RF performance.

For the RF measurement of the Invar filter, Fig. 9 shows the measurement results before and after silver plating without any tuning. As can be observed, both measured responses exhibit a shift of the passband against their simulated counterparts. The frequency shift before and after silver-plating is 70 MHz and 80 MHz, respectively. The small discrepancy (10 MHz) in the shifts is attributed to thickness of the plated silver layer which is estimated to be 11 µm. The conductivity of the Invar used in the simulation is extracted from the resonator measurement as given in Table IV.

For the silver-coated filter, the measured center frequency is 11.565 GHz, and the average insertion loss is around 1 dB, which is higher than the simulated one of 0.4 dB, as shown in Fig. 9(b). This extra loss is partly due to the lower-than-expected return loss (~10 dB) and partly due to the surface roughness [18], which degrades the effective conductivity of silver.

In the ideal situation of the resonator with infinite Q_u, the return loss of 10 dB alone would have contributed 0.45 dB mismatch loss. If perfectly smooth silver is assumed for the conductivity of the filter (6.302×10^7 S/m), the total insertion loss would be 0.8 dB. The Q_u can be calculated to be about 12500. For the measured insertion loss of 1 dB, the coupling matrix method is used to reproduce the measured response and to extract the corresponding Q_u. Fig. 9(c) shows a comparison between the measured result and the extracted filter response. They agree very well. From this figure, the Q_u can be extracted to be 5800, which is about 46% of the ideal silver-plated filter. Simulation shows this corresponds to an effective conductivity of 1.26×10^7 S/m. If the return loss can be improved to 15 – 20 dB, the insertion loss should be reduced to well under 1 dB. The higher-than-simulated S_{11} is probably due to the small dimension inaccuracies in critical coupling structures. Considering the narrow bandwidth and tuning-free measurement condition, we think the performance of the 3-D printed Invar filter is very encouraging.

To investigate the frequency shift of the passband which is believed to be mainly due to the material shrinkage during the printing process, a parameter study involving dimension scaling was carried out. The shrinkage ratio along *Z*-axis is set as *Sz* and that along the *XY*-plane is *Sa* (the shrinkage assumed to be isotropic along *X*/*Y* direction). As can be observed from Fig. 10, the shrinkage on *XY*-plane has a more pronounced effect on the frequency, while the *Z*-axis shrinkage incurs a small asymmetry to the transmission response, which also exists in the measurement result. Fig. 11 shows a comparison between the measured and simulated filter performance where $Sz = 0.99$ and $Sa = 0.995$. A reasonably good agreement can be observed.

Based on the above discussion, it is expected that the final filter performance can be improved by pre-design

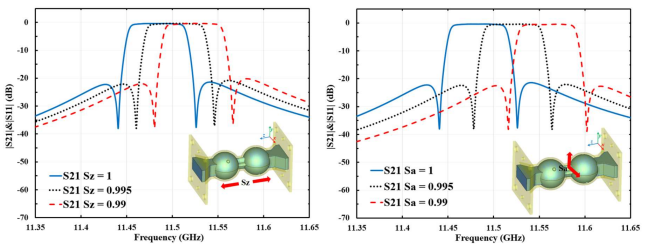

(a) (b)

Fig. 10. The simulated transmission response as a function of the shrinkage ratio. (a) shrinkage along the *Z*-axis. (b) Shrinkage along the *XY*-plane.

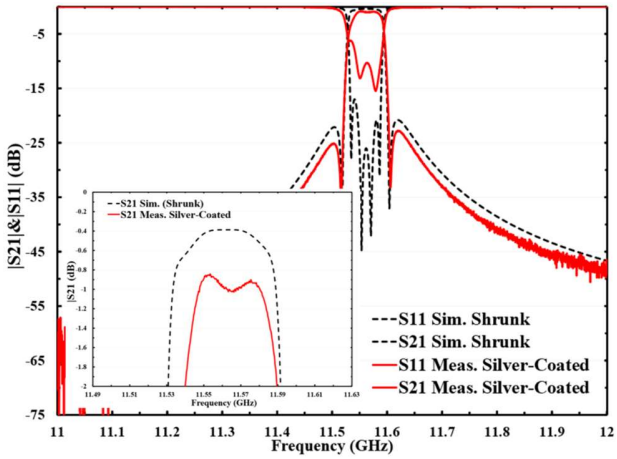

Fig. 11. Comparison of the filter performance. (Solid line: measurement result. Dot line: Simulation result considering the impact of shrinkage).

compensation for the dimension and by adding tuning screws.

To demonstrate this, holes were drilled on the 3D printed filter and six M2 stainless steel tuning screws were added for fine tuning the resonant frequencies and inter-resonator couplings. An improvement has been evidenced as shown in Fig. 12(a). However, the insertion loss with tuning screws is increased by almost 0.5 dB, as a result of loose installation of the screws as well as the loss from the un-plated steel materials. The corresponding Q_u can be extracted to be 2900 using the coupling matrix method, as shown in Fig. 12(b). It is expected that the insertion loss can be improved using silver-coated brass or Invar screws. It is also worth pointing out that a more optimal process is to drill the tuning holes before silver plating to avoid potential damage to the coating.

Next, the temperature-dependent RF measurement was performed on the Invar filter. The experiment process is similar to the resonator-based test. Fig. 13 shows the measured performances of the Invar filter. The temperature stable performance is clearly demonstrated. There is no visible frequency shift. The loss degradation at raised temperatures is 0.3 dB. It is worth noting that the thermal isolator pair, used in the thermal-RF measurement, contributes an extra insertion loss of 0.25 dB.

Table V provides a comparison with the 3-D printed A20X filter and an Invar filter fabricated by conventional CNC milling. There are two values given for the 3-D printed Invar filter, which correspond to the before/after-tuning results. The comparison shows that the added steel tuning screws not only increase the insertion loss but also degrade the thermal stability slightly. This could be alleviated by using silver-plated Invar screws. What is encouraging about the data is that the 3-D printed Invar filter (after tuning) exhibits comparable stability with the CNC Invar filter. The higher insertion loss can be accounted for by the low return loss as well as losses associated with the surface roughness and tuning screws.

TABLE V
SUMMARY AND COMPARISON OF THERMAL-RF MEASUREMENT RESULT.

	Insertion loss at ambient (dB)	Loss Degradation (dB)	Freq. temp. coefficient (ppm/K)
3-D Invar	1/1.5	0.2/0.3	0.5/1.1
3-D A20X	1.5	0.1	20
CNC Invar [1]	0.5	0.1	< 2

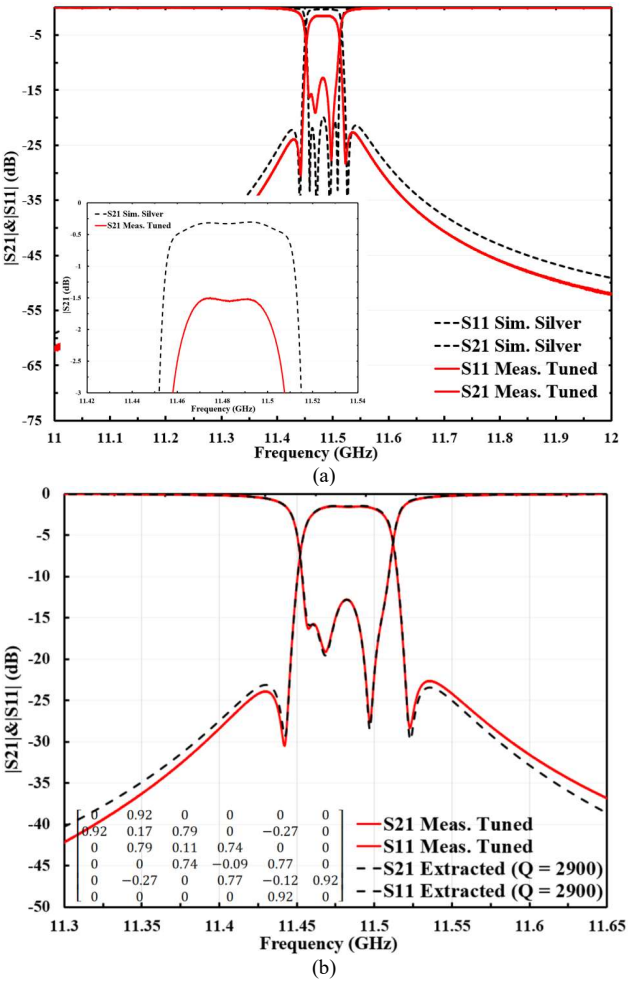

Fig. 12. (a) Measured and simulated results of the Invar filter after tuning with inset showing the enlarged view of the S_{21} over the passband. (b) Comparison between the measured results and the filter response from the extracted coupling matrix.

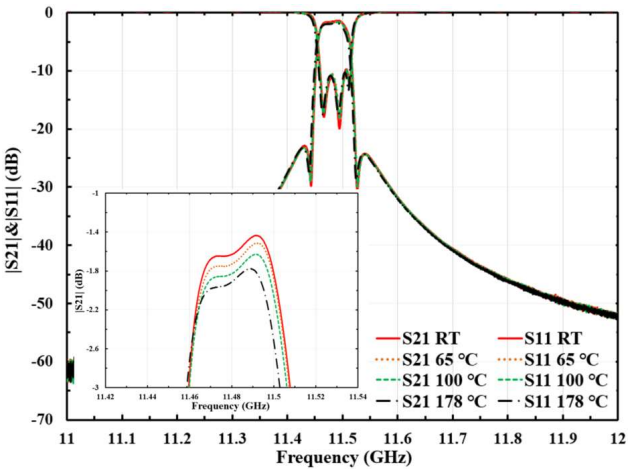

Fig. 13. Measured filter performances of the Invar filter after-tuning as a function of the temperature with inset showing the enlarged view of S_{21} over the passband.

TABLE VI
A COMPARISON WITH SOME 3-D PRINTED FILTERS AND CNC-MACHINED INVAR FILTERS.

Ref.	Filter Order and Resonator Type	f_c (GHz)	FBW (%)	Printing Technology	Material
[19]	4th-order, with mushroom-shaped coaxial resonators	7.924	3.9	SLM	Stainless steel
[20]	9th-order, with depressed super ellipsoid resonator	12.875	1.9	SLM	Scalmalloy aluminum alloy
[21]	3rd-order, with spherical resonator	10	1	SLM/SLA	Al-Cu alloy/Accura Xtreme resin
[12]	4th-order, with spherical dual-mode resonator	10	3	SLA	Accura Xtreme resin
[22]	4th-order, with dual-mode super Q resonator	19.9	0.22	CNC	Invar
T.W.	4th-order, with spherical dual-mode filter	11.483	0.47	SLM	Invar

Ref: reference, f_c: central frequency, FBW: fractional bandwidth; SLM: selective laser melting; SLA: stereolithography apparatus; CNC: computer numerical control; T. W.: this work.

V. CONCLUSION

A fourth-order 0.47% bandwidth spherical dual-mode filter designed for OMUX has been reported. To the best of our knowledge, this is the first demonstrated narrowband filter additively manufactured from Invar alloy in the open literature. Table VI provides a comparison with published 3-D printed filters and CNC Invar filters. This work demonstrates the possibility of using complex resonator structures in Invar filter design (without being limited to the rectangular and cylindrical cavities), and opens more design opportunities for optimal RF, mechanical and thermal properties for narrowband filters. The improvement in the thermal stability demonstrates the feasibility and superiority of the 3-D printed Invar filter. The end-to-end manufacturing methods and the detailed experimental investigation have been discussed. The presented design concept, manufacturing parameters, and material characterization may find useful applications in the design of future high-power filters.

The 3D-printed Invar filter technology is not without challenges. Conventional machined Invar filters of the similar fractional bandwidth can have an insertion loss as low as 0.5 dB. To match this performance, more work needs to be done about the surface treatment (polishing and coating). Polishing the internal surface of monolithically-built closed cavity is especially challenging. Currently we are restricted to vibratory grinding technique, which is less intrusive to the internal critical structures compared with some other more aggressive polishing methods but also has limited capability. Electrochemical polishing may be a promising alternative. The quality of silver plating on the SLM Invar filter can be improved. Reducing the surface roughness will help. It is worth mentioning that to understand the 3D printed internal surfaces is an ongoing research area. The influence of multiple factors such as the laser process parameters, the printing direction and the thermal treatment complicates this matter significantly. Finally, it is also expected more weight reduction features, and further optimized resonator geometry are expected to enhance the competitiveness of the SLM Invar technology in high-power filter applications.

REFERENCES

[1] B. Yassini and M. Yu, "Ka-band dual-mode Super Q filters and multiplexers," *IEEE Trans. Microw. Theory Tech.*, vol. 63, no. 10, pp. 3391–3397, 2015.

[2] M. Yu, D. J. Smith, A. Sivadas, and W. Fitzpatrick, "A dual mode filter with trifurcated iris and reduced footprint," *IEEE MTT-S Int. Microw. Symp. Dig.*, vol. 3, pp. 1457–1460, 2002.

[3] M. D'Auria *et al.*, "3-D Printed Metal-Pipe Rectangular Waveguides," *IEEE Trans. Components, Packag. Manuf. Technol.*, vol. 5, no. 9, pp. 1339–1349, 2015.

[4] X. Shang, J. Li, C. Guo, M. J. Lancaster, and J. Xu, "3-D printed filter based on helical resonators with variable width," *IEEE MTT-S Int. Microw. Symp. Dig.*, pp. 1587–1590, 2017.

[5] M. Salek, X. Shang, and M. J. Lancaster, "Compact S-Band Coaxial Cavity Resonator Filter Fabricated by 3-D Printing," *IEEE Microw. Wirel. Components Lett.*, vol. 29, no. 6, pp. 382–384, 2019.

[6] V. E. Boria and B. Gimeno, "Waveguide filters for satellites," *IEEE Microw. Mag.*, vol. 8, no. 5, pp. 60–70, 2007.

[7] A. E. Williams, "A Four-Cavity Elliptic Waveguide Filter," *IEEE Trans. Microw. Theory Tech.*, vol. 18, no. 12, pp. 1109–1114, Dec. 1970.

[8] S. Cogollos *et al.*, "A systematic design procedure of classical dual-mode circular waveguide filters using an equivalent distributed model," *IEEE Trans. Microw. Theory Tech.*, vol. 60, no. 4, pp. 1006–1017, 2012.

[9] C. Qiu, N. J. E. Adkins, and M. M. Attallah, "Selective laser melting of Invar 36: Microstructure and properties," *Acta Mater.*, vol. 103, pp. 382–395, 2016.

[10] C. Guo, J. Li, X. Shang, M. J. Lancaster, and J. Xu, "Progress on microwave devices fabricated using stereolithography 3-D printing technique," *2017 Int. Appl. Comput. Electromagn. Soc. Symp. China, ACES-China 2017*, no. 2, pp. 2–3, 2017.

[11] C. Tomassoni, O. A. Peverini, G. Venanzoni, G. Addamo, F. Paonessa, and G. Virone, "3D Printing of Microwave and Millimeter-Wave Filters: Additive Manufacturing Technologies Applied in the Development of High-Performance Filters with Novel Topologies," *IEEE Microw. Mag.*, vol. 21, no. 6, pp. 24–45, Jun. 2020.

[12] C. Guo, X. Shang, J. Li, F. Zhang, M. J. Lancaster, and J. Xu, "A Lightweight 3-D Printed X-Band Bandpass Filter Based on Spherical Dual-Mode Resonators," *IEEE Microw. Wirel. Components Lett.*, vol. 26, no. 8, pp. 568–570, 2016.

[13] J.-S. Hong and M. J. Lancaster, *Microstrip Filters for RF/Microwave Applications*. New York, USA: John Wiley & Sons, Inc., 2001.

[14] L. N. Carter *et al.*, "Process optimisation of selective laser melting using energy density model for nickel based superalloys," *Mater. Sci. Technol. (United Kingdom)*, vol. 32, no. 7, pp. 657–661, 2016.

[15] X. Li *et al.*, "Improved plasticity of Inconel 718 superalloy fabricated by selective laser melting through a novel heat treatment process," *Mater. Des.*, vol. 180, 2019.

[16] J. Hesler, A. R. Kerr, and N. Horner, "A broadband waveguide thermal isolator," *14th Int. Symp. Sp. Terahertz Technol.*, pp. 148–154, 2003.

[17] C. Guo *et al.*, "Shaping and Slotting High-Q Spherical Resonators for Suppression of Higher Order Modes," *IEEE MTT-S Int. Microw. Symp. Dig.*, vol. 2019-June, pp. 1205–1208, 2019.

[18] G. Gold and K. Helmreich, "A physical surface roughness model and its applications," *IEEE Trans. Microw. Theory Tech.*, vol. 65, no. 10, pp. 3720–3732, 2017.

[19] S. W. Sattler, F. Gentili, R. Teschl, and W. Bösch, "Direct Metal Printed 4th order Stepped Impedance Filter in the C/X Band," *IEEE MTT-S Int. Microw. Symp. Dig.*, vol. 2018-June, pp. 145–148, 2018.

[20] P. A. Booth and E. Valles Lluch, "Realising advanced waveguide bandpass filters using additive manufacturing," *IET Microwaves,*

Antennas Propag., vol. 11, no. 14, pp. 1943–1948, 2017.
[21] F. Zhang *et al.*, "3-D Printed Slotted Spherical Resonator Bandpass Filters with Spurious Suppression," *IEEE Access*, vol. 7, pp. 128026–128034, 2019.
[22] B. Yassini and M. Yu, "A novel ka band dual mode super Q Cavity Filter," *IEEE MTT-S Int. Microw. Symp. Dig.*, pp. 220–222, 2014.

Lu Qian (Graduate Student Member, IEEE) was born in Hunan, China. He received the B.Eng. degree (Hons.) in information engineering and M.S. degree in information and communication system from South China University of Technology, Guangzhou, China, in 2016 and 2019, respectively. He is currently pursuing the Ph.D. degree in electronic and electrical engineering at the University of Birmingham, Edgbaston, Birmingham, U.K.

His current research interests include microwave filters, multi-port coupled resonator networks, 3-D printed high-power microwave devices.

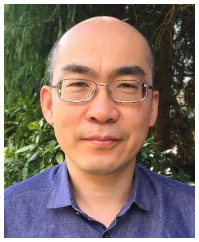

Yi Wang (Senior Member, IEEE) was born in Shandong, China. He received the B.Sc. degree in applied physics and M.Sc. degree in condensed matter physics from the University of Science and Technology, Beijing, China, in 1998 and 2001, respectively, and the Ph.D. degree in electronic and electrical engineering from the University of Birmingham, Edgbaston, Birmingham, U.K., in 2005.

From 2004 to 2011, he was a Research Fellow at the University of Birmingham. In 2011, he became a Senior Lecturer and then Reader at the University of Greenwich, U.K., He is currently Associate Professor with the University of Birmingham. He is the author of over 180 research papers and has been the reviewer of several major microwave, antenna and sensor journals and an Associate Editor of IET MAP. He serves the TPC Chair of 2021 European Microwave Conference. His current research interests include multiport filtering networks, filter-antenna integration, millimeter-wave and terahertz antennas and devices for metrology, communication, and sensing. He is particularly interested in working with new materials and novel manufacturing techniques, such as micromachining and 3D printing, for RF/microwave applications.

Sheng Li received Ph.D. degree in Materials Science from University of Birmingham, UK, in 2017. He is currently working as a lecturer in the School of Electromechanical Engineering, Guangdong University of Technology.

He is the author of 26 research publications. His research interests include additive manufacturing of metal and ceramic, processing and microstructure of shape memory alloys, Ni superalloys, Ti alloys, Al alloys and metal matrix composite. He has worked on the projects supported by leading companies across the world including Rolls-Royce, Airbus, Honda, BAE Systems, MBDA Missiles, MicroTurbo, Ford, and European Space Agency.

Abd El-Moez A. Mohamed received a PhD on "Functional magnetic materials and their application in magnetism sensing and refrigeration" in 2017 from the University of Oviedo, Spain. Then after he joined the Advanced materials processing lab (AMPLab) at the University of Birmingham, United Kingdom, as a research fellow. His main research is additive manufacturing of functional magnetic materials and their application in magnetic shielding, magnetic sensing and magnetic refrigeration, with supporting other additive manufacturing projects.

Moataz M. Attallah received his PhD in metallurgy and materials science from the University of Birmingham in 2007. He holds a chair in advanced materials processing at the School of Metallurgy and Materials University of Birmingham. His research focuses on developing a metallurgical understanding of the material-process interaction in additive manufacturing of metallic materials focusing on the process impact on the microstructure and structural integrity development. His research is conducted through research partnerships with various companies in the aerospace, defense, medical, space, and nuclear energy sectors. He co-authored over 150 journal and conference papers, 3 book chapters, and is a co-inventor on 8 patent applications.

Talal Skaik received M.Sc. degree in communications engineering and Ph.D. degree in microwave engineering from the University of Birmingham, Birmingham, U.K., in 2007 and 2011, respectively.

After PhD, he worked in lecturing in electrical engineering until 2019. He is currently working as a research fellow in the Electronic, Electrical and Systems Engineering Department at the University of Birmingham. His research interests include microwave filters and antennas, 3D-printed microwave devices, temperature compensated filters for satellite payloads, multi-port coupled resonator structures and energy harvesting circuits.

Paul Booth received the B.Eng. degree in electrical engineering from the University of Leeds, UK, in 1987.

From 1987 to 1994 he worked at BAe Space Systems on LNAs, SSPAs, filters and multiplexers. From 1994 to1995 he worked for Phase Devices Ltd on mobile base station filters and diplexers. From 1995 to 1998 he worked at Matra Marconi

Space as Responsible Engineer on a number of filters and multiplexers. In 1998 he moved to Ericsson Radio Access, Stockholm, Sweden, where he was responsible for the design of mobile comms. passive RF equipment. Since 2003 he has been at Airbus Defense and Space, Stevenage, UK where he is currently working in the Antenna Group. His research interests include filter design, modelling and realization, high power phenomena and novel manufacturing techniques.

Laurent Pambaguian received a PhD on "Mechanical behaviour of interfaces in Metal Matrix Composites" in 1994 from ONERA, The French Aeronautic Lab. He did two post docs in Spain on heterogeneous deformation of aluminium alloys and in Austria on metal matrix composites. In 1999 he has been recruited as Engineer in the Materials and Processes Section of the European Space Agency and focused on addressing the development of advanced materials and processes for the future ESA missions. He has been the first to develop Additive Manufacturing Technologies at ESA and is expanding his expertise on this topic since 2004.

César Miquel-España was born in València, Spain. He received the Licenciado degree (Hons.) in Physics and PhD degree in Theoretical Physics from the Universitat de València, Spain in 2002 and 2008 respectively. He is currently working at the European Space Agency in Noordwijk, NL.

His current research interests include microwave filters, ferrite devices, additive manufacturing and high power RF phenomena.

Petronilo Martín-Iglesias (Member, IEEE) was born in Caceres, Spain, on April 23, 1980. He received the Telecommunication Engineering degree from the Polytechnic University of Madrid, Madrid, Spain, in 2002, and the Master degree from The University of Leeds, Leeds, U.K., in 2012.

He has been working in industry for over ten years as a Microwave Engineer involved with active (high power amplifiers for radar applications) and passive (filters, multiplexers, couplers, etc.) RF hardware design, including two years as a Radar System Engineer with Indra Sistemas, ISDEFE S.A., and Thales Alenia Space Spain. Since Summer 2012, he has been involved with research and development and project support activities related with RF passive hardware developments for the European Space Agency. His research interests are filter synthesis theory, electromagnetic (EM) design and high power prediction, as well as advanced manufacturing techniques for RF passive hardware. From January 2021 he is part of the Earth Observation Future Microwave Instruments Section at ESA-ESTEC.